Optical Activity Enhanced by Strong Inter-molecular Coupling in Planar Chiral Metamaterials

Teun-Teun Kim[1]*†, Sang Soon Oh[2]*, Hyun-Sung Park[1], Rongkuo Zhao[2], Seong-Han Kim[3], Wonjune Choi[4], Bumki Min[1] & Ortwin Hess[2]

[1]Department of Mechanical Engineering, Korea Advanced Institute of Science and Technology(KAIST), Daejeon 305-701, Republic of Korea, [2]The Blackett Laboratory, Department of Physics, Imperial College London, South Kensington Campus, London SW7 2AZ, United Kingdom, [3]Advanced Photonics Research Institute, GIST, Gwangju, 500-712, Republic of Korea, [4]Department of Physics, Korea Advanced Institute of Science and Technology (KAIST), Daejeon 305-701, Republic of Korea.

The polarization of light can be rotated in materials with an absence of molecular or structural mirror symmetry. While this rotating ability is normally rather weak in naturally occurring chiral materials, artificial chiral metamaterials have demonstrated extraordinary rotational ability by engineering intra-molecular couplings. However, while in general, chiral metamaterials can exhibit strong rotatory power at or around resonances, they convert linearly polarized waves into elliptically polarized ones. Here, we demonstrate that strong inter-molecular coupling through a small gap between adjacent chiral metamolecules can lead to a broadband enhanced rotating ability with pure rotation of linearly polarized electromagnetic waves. Strong inter-molecular coupling leads to nearly identical behaviour in magnitude, but engenders substantial difference in phase between transmitted left and right-handed waves.

Since its discovery, optical activity has been widely utilized in many fields of science including chemistry, physics, biology, and optics[1]. It can be measured by the rotation angle of the plane of linearly polarized light[2] and is generated in a material with a chiral internal structure lacking mirror symmetry[3]. While naturally chiral materials such as DNA, sugar and many other bio-molecules display only rather modest optical activity, artificial chiral metamaterials comprised of sub-wavelength metallic resonators have recently been shown to exhibit large optical activity[4–6]. On top of this, chiral metamaterials are also of particular interest for negative refraction[7–11], the Casimir effect[12], strong nonlinear optical activity[13], polarization switching and modulation[14,15] as well as various other applications such as broadband circular polarizers and wave plates[16–19]. Therefore, significant efforts have been devoted to conceiving and demonstrating various designs of chiral metamaterials for enhanced chirality, including conjugated gammadions[20] and double four-U structures[21]. Strong chirality of various artificial chiral structures has been tested experimentally, which is also theoretically supported by a model taking intra-molecular couplings into consideration[22,23]. Yet, despite the remarkable possibility of achieving strong chirality, very large ellipticity at resonances remains an obstacle for potential applications of chiral materials as incident linear polarization states become elliptically polarized after being transmitted through the media. Moreover, with only the concept of intra-molecular coupling, the value to which the optical activity can be enhanced is limited and governed by morphological shaping or arrangement of metamolecules so that a degree of freedom in design methodology for chiral metamaterials is seriously restrained.

Here, we experimentally and theoretically demonstrate a new class of bi-layer metamaterial structures that substantially enhance optical activity through strong *inter-molecular* coupling between adjacent planar chiral metamolecules. This structure, a conjugated double Z metamaterial (CDZM), can maximize inter-molecular capacitive coupling to achieve its remarkable optical activity. On the basis of a semi-analytic coupled RLC resonator model and numerical simulations, we explain qualitatively and quantitatively how the observed optical activity scales with the width of the gap between adjacent planar metamolecules in the CDZM. We show that a strong inter-molecular coupling not only leads to enhanced chirality but also to reduced ellipticity at resonant frequencies.

In order to fully exploit the strong inter-molecular capacitive coupling, we designed the CDZM as depicted in Fig. 1a by morphologically transforming a conventional conjugated gammadion structure[20] (See Method). The conjugated arrangement of the CDZM maintains resonant chiral properties of the conjugated gammadion
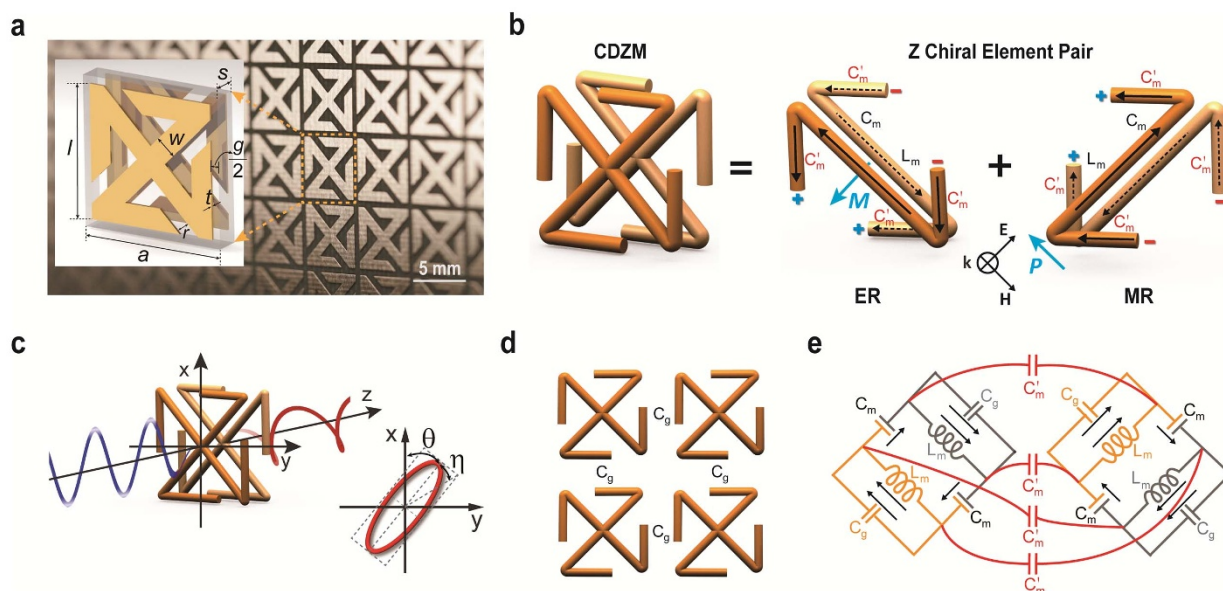
Figure 1 | Conjugated double Z metamaterial and an equivalent RLC model (a) Schematic view of the unit cell structure and photograph of the CDZM sample with the dimensions indicated in the figure: $l = 5.5$ mm, $w = 0.9$ mm, $s = 0.5$ mm, $r = 0.6$ mm, and the thickness of the copper $t = 18$ μm. The gap width between chiral metamolecules is defined by $g = a - l$. (b) Schematics of the equivalent RLC model for the CDZM. C'_m is the capacitances of the side strips and L_m and C_m are the inductance and capacitance of the central strips respectively. The incident electric field (**E**) induces the surface current in the central strip (black arrow) resulting in magnetization (**M**) and, similarly, the electric charges (represented by +, −) driven by the magnetic field (**H**) induces electric polarization (**P**). (c) Ellipticity angle η and azimuthal rotation angle θ represent the polarization state of the transmitted electromagnetic waves. (d) Schematics of CDZM arrays. C_g is the gap capacitance which represents additional inter-molecular coupling between metallic strips in neighbouring unit cells. (e) Equivalent RLC circuits for Z chiral element pairs. For simplicity, the resistor elements have been omitted. The arrow indicates the current direction.

structure that exhibits two distinct fundamental resonances in the low frequency range. However, in contrast to the conjugated gammadion structure, each arm of the CDZM is constructed in such a way that a small lateral gap of width g is maintained between adjacent chiral metamolecules for strong capacitive coupling. It can therefore be predicted that g (Fig. 1a) will play a critical role in enhancing the effective chirality parameter in the CDZM. In close analogy to the case of high index metamaterials that utilize strong capacitive coupling[24], an effective chirality parameter is expected to scale differently in weak and strong inter-molecular coupled regimes.

The physical mechanism of optical rotation of CDZM is similar to the one in a type of bilayer chiral metamaterials such as gammadion structures[20]. For simplicity, the unit cell of CDZM can be decomposed into conjugated Z chiral element pairs as shown in Fig. 1b. Upon a linearly polarized electromagnetic excitation, the external electric field (**E**) induces an antiparallel current in the central strips resulting in a magnetization (**M**) in the direction opposite to the incident electric field. Similarly, electric charges driven by the magnetic field (**H**) result in an electric polarization (**P**) in the direction opposite to the incident magnetic field. Thus, the coupling between the electric and magnetic fields in the unit cell of a CDZM rotates the polarization plane of linearly polarized light by the azimuthal angle θ as shown in Fig. 1c. This coupling effect can be described by employing an equivalent RLC model. From our simulation results (see Supplementary Information Section SI for field distributions at resonances) we can assign inductive and capacitive coupling elements L_m, C_m, and C'_m (see Fig. 1b). However, it should be noted that, in contrast to bilayer chiral metamaterials demonstrated so far, CDZM exhibit additional strong capacitive coupling between adjacent metamolecules (C_g) shown in Fig. 1d. This characteristic CDZM coupling can be classified as intra-molecular (L_m, C_m and C'_m) and inter-molecular (C_g) couplings. Here, the intra-molecular coupling refers to capacitive (charge-to-charge) and inductive (current-to-current) coupling between metallic strips in one unit cell and the inter-molecular coup-

ling refers to the coupling between metallic strips in neighbouring unit cells (see Supplementary Information Section SII for details of intra-molecular coupling for CDZM).

To understand this novel coupling property, let us first focus on the role of the inter-molecular coupling C_g in enhancing optical activity. For gap widths comparable to the width of metallic strips w ($g \approx w$), C_g is much smaller than C_m and C'_m since the area per unit length facing each other in C_g is smaller than the ones in C_m and C'_m ($t \ll w$). Therefore, the contribution of C_g to the current induced in the central strips can be ignored. In contrast, when the gap is comparable to t or smaller than t ($g \lesssim t$), C_g can be increased to a value comparable to C_m and C'_m or even to an extremely large value since C_g is inversely proportional to the gap width. The increase of capacitance implies that more charge can be accumulated in C_g so that it allows more current to flow in the central strips. As a result, optical activity is enhanced by reducing the gap width. It is worth to point out that the enhancement of optical activity is not restricted to resonant frequencies since the enhanced inter-molecular coupling exists for a wide frequency range[25].

To obtain an understanding of the nature and relative role of intra- and inter-molecular coupling, we use a coupled RLC model. As shown in Fig. 1e, each Z chiral element pair in one unit cell is represented by one equivalent RLC circuit and the unit cell is represented by a coupled RLC resonator. For simplicity, the resistor elements have been omitted. It should be noted that the RLC resonators are similar to the one for cut-wire pairs[26]. By analysing the equivalent RLC circuit, we note that the coupled RLC resonator is, in fact, a combination of three resonators that all share one inductance L_m but are individually distinguished by separate constituting capacitances C_m, C'_m and C_g, respectively. From the equations of motion for the electric charge, we obtain expressions for the resonance frequencies $f_{1,2}$ and the effective chirality parameter of the CDZM (see Supplementary Information Section SI for resonance frequencies of CDZM). The resonance frequencies for the CDZM are given as

$$f_1 = \frac{1}{2\pi\sqrt{L_m C_m}} \times \sqrt{1 + x - \sqrt{1 + x^2}} \quad \text{where} \quad x = C_m/(C_m' + C_g) \quad \text{and}$$

$$f_2 = 1 \Big/ \left(2\pi\sqrt{L_m(C_m' + C_g)} \right) \quad \text{for MR and ER, respectively. As can}$$

be confirmed from the expression, the resonance frequency shift for the variation in gap width depends solely on the inter-molecular coupling C_g, because the intra-molecular couplings C_m and C_m' are independent of the gap width g. Moreover, the effective chirality parameter is expressed with the chiral resonance strength[27], which is inversely proportional to $f_{1,2}$. Therefore, the optical activity is proportional to the square root of the capacitance of the Z element (see Supplementary Information Section SI for the effective chirality parameters of CDZM).

To shed further light on the chiral response of a CDZM in the regime of strong inter-molecular coupling, we focus on the scaling behaviour of the gap capacitance C_g of the Z element with the gap width g. Using a coplanar strip capacitance formula[28], the gap capacitance C_g can be expressed as

$$C_g \simeq \varepsilon_0 \varepsilon_r \left\{ 1.15 \left(\frac{2t}{g} \right) + 2.80 \left(\frac{2w}{g} \right)^{0.22} \right\} l_e, \text{ with the vacuum permit-}$$

tivity ε_0, the relative permittivity of the substrate material ε_r, the thickness of the strip t, the effective length of the side strip l_e and its width w. As can be seen in Fig. S3, three regimes of capacitive coupling are delineated according to the scaling behaviour with the gap width: (1) an intra-molecular coupling regime where the resonance frequencies $f_{1,2}$ remain almost constant, (2) a weak inter-molecular coupling regime where $f_{1,2}$ decreases with a rate of $g^{0.11}$, and (3) a strong inter-molecular coupling regime where $f_{1,2}$ is proportional to $g^{1/2}$. In the strong inter-molecular coupled regime, one obtains the relation $\Omega_\kappa \propto g^{-1/2}$ between resonant strength coefficients and g (see Supplementary Information Section SI for definition of the three regimes of coupling) resulting in a significant increase of the chirality parameter κ at pure optical activity (i.e., the transmitted wave remains linearly polarized with rotation angle θ) as g becomes very small.

To examine the optical activity of the CDZM, we follow a well-established characterization approach[22,27]. The measured transmission amplitudes and phases for the RCP and LCP waves through the CDZM are shown in Fig. 2 with a variation in gap width g from 0.1 to 5 mm. As expected from the conjugated design, two strong resonances appear in both transmission amplitude and phase spectra at the frequencies f_1 and f_2. For the off-resonance frequencies, the transmission amplitudes for the RCP and LCP waves are nearly indistinguishable, which implies that the ellipticity is very small. For the resonance frequencies, the difference in transmission amplitudes for the RCP and LCP waves is significantly reduced as the gap width becomes smaller. In contrast, the phase spectra differ significantly near the resonance frequencies, which is clear evidence of the gigantic optical activity of the CDZM (Fig. 2). More interestingly, in the strong inter-molecular coupled regime (for the case of $g = 0.1$ mm), the phase difference becomes even larger not only at the resonances but also between the resonances. This suggests that broadband enhanced optical activity is attainable by strong inter-molecular coupling. In addition, the resonance frequencies f_1 and f_2 are red-shifted with decreasing g, which is consistent with the coupled RLC model. Here, geometrical parameters are chosen such that the resonance frequencies are positioned in the frequency range between 7 and 13 GHz. However, it is worthwhile to note that the concept can be extended to other frequency ranges (see Supplementary Information Section SIV for CDZM at THz frequencies).

To see how the optical activity scales in different coupling regimes, the chirality parameter κ (Fig. 3a) and ellipticity η (Fig. 3b) are estimated (solid line) from the transmission spectra (Fig. 2) and compared with numerically calculated values (circles) for several values of gap width g. In the strong inter-molecular coupling regime, the ellipticity becomes practically negligible ($\eta \approx 0$) in a broad frequency range
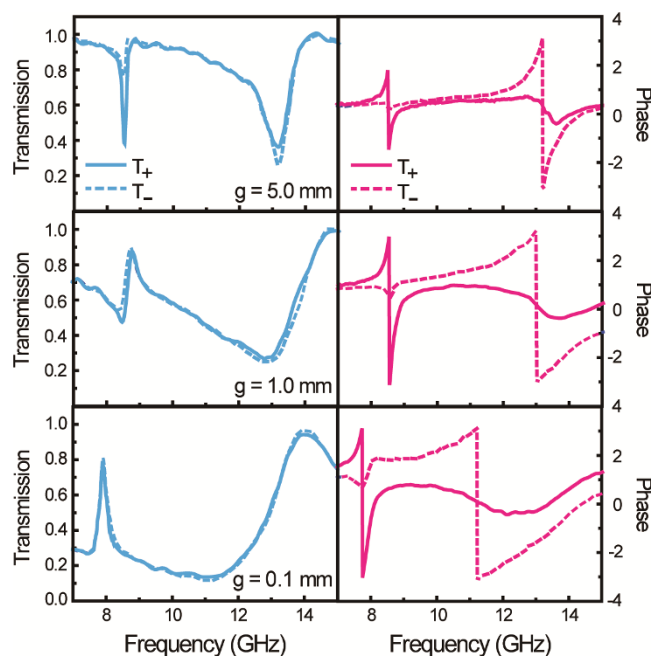

Figure 2 | Gap-dependent amplitude and phase changes of waves transmitted through the CDZM. Measured transmission spectra and phases of right-handed circularly polarized (RCP, solid line) and left-handed circularly polarized (LCP, dashed line) waves are plotted for different gap widths g. While the transmission difference between RCP and LCP waves is very small due to the small absorption, the phase difference is significant due to the large optical activity.

between the two resonances, where a substantial amount of pure optical activity can still be observed (highlighted by blue dashed line in Fig. 3d). In this broad frequency range, linearly polarized waves maintain their linearity while being rotated by an angle θ when passing through CDZM. The frequency region of small ellipticity is bounded by the two resonance frequencies where the ellipticity increases due to increased absorption. We note that while a zero-ellipticity frequency, at which the ellipticity becomes zero, is a common feature of bi-layer chiral metamaterials which have two resonances[23], the optical activity at that frequency is generally not large enough. Figures 3c,d show simulated values of κ and η as a function of gap width g. The red shift of the resonant frequencies for smaller gap width can be clearly observed, which is consistent with our coupled RLC model above.

In order to compare the effective parameters at the frequency of pure optical activity, Fig. 3e shows the dependence of the chirality parameter κ at $\eta = 0$ on the gap width. Theoretical chirality parameters κ obtained from the coplanar strip capacitance formula are also plotted in Fig. 3e (see Supplementary Information for details) as well as the theoretical chirality parameter as obtained from the coplanar strip capacitance formula (blue line). As mentioned above, in the strong inter-molecular coupling regime (red shaded region), the chirality parameter κ is proportional to $g^{-1/2}$ and increases even more rapidly than that in the weak inter-molecular coupled regime (blue shaded region). In the strong inter-molecular coupled regime ($g = 0.1$ mm), we experimentally achieved very large value of the chirality parameter $\kappa = 6.2$ (6.5 in the simulation results) at $f_{\eta=0}$. This corresponds a rotation angle θ of 31.4° at $f_{\eta=0} = 9.0$ GHz, which means that the rotation angle per wavelength reaches $1933°/\lambda$. Here, the thickness of the sample is 0.536 mm. Simulation results in Fig. 3e show that the chirality parameter can reach up to 28 for $g = 0.5$ µm.

Moreover, as the gap becomes smaller, the ellipticity η significantly decreases not only at non-resonant frequencies but also at the resonance frequency (Fig. 3f). The theoretical scaling property of the ellipticity $\eta \propto 1/C_g$ (blue line) shows an excellent agreement with
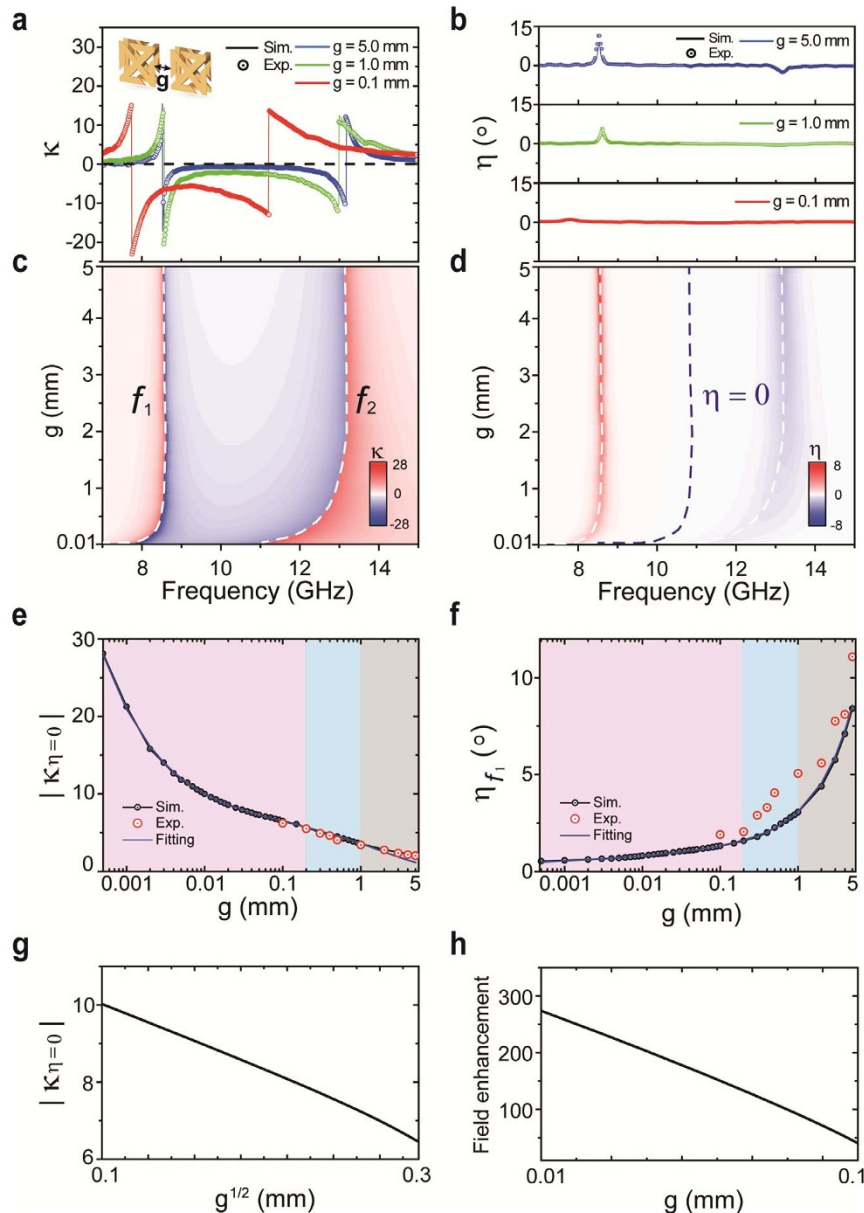
Figure 3 | Effective parameters as a function of the gap width for the CDZM. Comparisons are made between simulated (solid lines) and measured (circles) (a) chirality κ and (b) ellipticity η for different gap widths g. Simulated effective parameters (c) chirality κ and (d) ellipticity η are plotted with the gap width g ranging from 10 μm to 5 mm. The white dashed lines represent the frequencies f_1 and f_2, and the blue dashed line represents the region of pure optical activity, $\eta = 0$. (e) The chirality κ at the frequencies for which $\eta = 0$ and (f) the ellipticity η at the resonant frequency f_1 as a function of the gap width g. The black circled line and the red scatters represent simulated and measured results, respectively. The theoretical fitting obtained from the coplanar strip capacitance formula is drawn as a blue line as a function of the gap width g. Three regimes of coupling (uncoupled: grey shaded; weak inter-molecular coupled: blue shaded; strong inter-molecular coupled: red shaded) regimes can be defined for the ranges of gap width. As the gap width decreases, κ increases significantly and η decreases. Comparison between the (g) chirality parameter $|\kappa_{\eta=0}|$ and (h) field enhancement factor with varying gap width g in the strong inter-molecular coupled regime.

simulation results and confirms that the near-zero ellipticity indeed is a result of the strong inter-molecular coupling and corresponding field localization effect. In the case of $g = 0.1$ mm, the ellipticity of the transmitted wave is less than $1.3°$ ($1.9°$ in the experimental results) across the whole frequency range of interest. Because of this substantial decrease in ellipticity, the transmitted waves at the resonant frequencies remain highly linearly polarized at a rotated angle θ for a linearly polarized incident wave. This is very important for practical applications since the resonance frequencies, where polarization rotation reaches the maximum $\theta = 90°$, can be used for polarization rotation, which has been impossible with conventional bilayer chiral metamaterials. We measured azimuthal rotation angles

θ as large as $88.7°$ at the resonance frequency $f_1 = 7.8$ GHz and $88.0°$ at $f_2 = 11.2$ GHz. These experimental results show that the rotation angle θ per wavelength reaches values in excess of $6288°/\lambda$ and $4383°/\lambda$ at f_1 and f_2, respectively.

To confirm that the enhanced optical activity originates from the strong inter-molecular coupling in the CDZM, we numerically calculated the electric field enhancement in the gap between the two metallic strips using geometric parameters consistent with those of our samples. The induced electric field is expected to increase for smaller gap widths due to an increased capacitance (see Methods). Full-wave electromagnetic simulations confirm electric field enhancements near the metallic strips of CDZM elements. The field
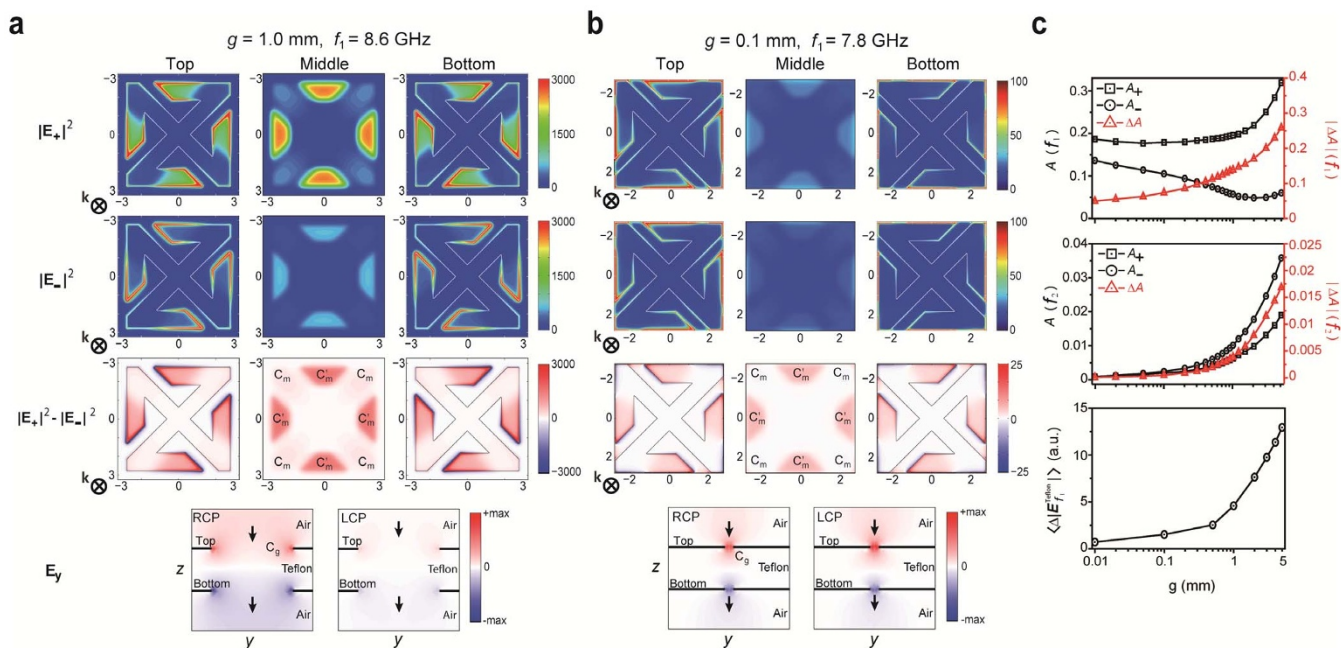
Figure 4 | Gap dependence of the electric field distribution and absorption. Electric field intensity distribution for RCP ($|E_+|^2$) and LCP ($|E_-|^2$), the difference of the electric field ($|E_+|^2 - |E_-|^2$) and horizontal electric field amplitude E_y for RCP and LCP in the CDZM with g equal to (a) 1.0 mm and (b) 0.1 mm at the resonance frequency f_1. Electric fields are confined in the region denoted as C_m and C'_m for $g = 1.0$ mm whereas the electric fields are more localized around the gap for $g = 0.1$ mm reducing the electric fields at C_m and C'_m significantly. As a result, the difference of the electric field ($|E_+|^2 - |E_-|^2$) for RCP and LCP waves reduces significantly. (c) Absorption A_+ (A_-) for RCP (LCP) and the absorption difference $|\Delta A|$ as a function of the gap width g at f_1 (top) and at f_2 (middle) and difference of the average field stored in the Teflon substrate for RCP and LCP as a function of g (bottom).

enhancement factor ($<E_{gap}>/E_{in}$) and retrieved chirality parameter $\kappa_{\eta = 0}$ with varying gap width g at resonance frequency $f_{\eta = 0}$ are shown in Figs. 3g,h. By reducing the gap width g, we can see that the enhancement factor and $\kappa_{\eta = 0}$ are proportional to g^{-1} and $g^{-1/2}$, respectively. These pronounced dependencies on the gap width strongly suggest that the enhancement of the optical activity originates from the small-gap effect (see Supplementary Information Section SV for Electric field profiles for CDZM).

The reduced ellipticity can equally be explained by the strong field localization in the gap and the corresponding decrease in absorption difference (the absorption difference $|\Delta A|$ is equal to the difference in transmission because the reflections of RCP and LCP waves are the same). The loss values of the CDZM can be attributed to dissipation in the lossy dielectric substrate as absorption in the metallic elements is negligible at microwave frequencies (see Supplementary Information Section SVI for details of possible loss channels in CDZM). To figure out where the absorption occurs in the CDZM, we plot the electric field intensity that is associated with absorbed power per unit volume ($p_{abs} = \frac{1}{2} \varepsilon_i \varepsilon_0 \omega |E_\pm|^2 \epsilon_i$ where ϵ_i is the imaginary part of the relative permittivity) for the RCP and LCP wave excitations. In the case of $g = 1.0$ mm (weak inter-molecular coupled regime), as shown in Fig. 4a, electric fields are confined mostly in the lossy dielectric substrates between the top and bottom metal strips of central and side arms (C_m and C'_m in the equivalent circuit); however, for $g = 0.1$ mm (strong inter-molecular coupled regime) shown in Fig. 4b, the electric fields become more confined to the air gap resulting in a smaller absorption difference for RCP and LCP. For the resonant frequency f_1 (Fig. 4c), the absorption for the RCP reduces and thereby the absorption difference $|\Delta A|$ decreases significantly. In addition, for the resonant frequency f_2, both the absorptions for the RCP and LCP waves reduces significantly thereby giving the much smaller absorption difference. In the bottom of Fig. 4c, the difference of the average electric field intensity in the Teflon substrate for RCP and LCP at the resonant frequency f_1 is displayed. As the figure

shows, the difference of the average electric field intensity decreases for smaller gap widths, which leads to a reduced ellipticity.

This allows us to conclude that our strong inter-molecular coupling approach in chiral metamaterials is inherently different from previous work where, e.g. coupling of resonances has been employed to engineer bandwidth[29-31]. First, the gap width g, represents an additional and key design parameter that allows us to control the enhancement continuously from a small value to an extremely large one. Second, the strong localization of fields in the small gap provides specific spatial positions where active materials or gain media can be incorporated[32] with an aim to tune and further enhance the chiral property of a chiral metamaterial efficiently. Although transmission amplitudes decrease as g becomes smaller (as low as 13% for the broad frequency range near the frequency f_2 in the case of $g = 0.1$ mm), it should be noted that the low transmission does not originate from a large absorption but it is caused by high reflection. Thus, by matching the impedance with a high permeability material or antireflective multiple layer structures, there are, in principle, various ways of increasing the transmission while maintaining large optical activity. This conceivably enables tuneable chiral metamaterials with a wide dynamic range and/or electrical pump switching of chirality.

Methods

Sample fabrication and measurement. The 18 μm thick copper patterned CDZM structures are fabricated on each sides of the Teflon board (Taconic TLX-9) with a thickness $s = 0.5$ mm by conventional printed circuit board technology. Transmission and reflection measurements were performed using a free-space measurement system with a network analyser (Agilent PNA-L) and two horn antennas (ETS Lindgren 3160), acting as source and receiver, respectively. In order to remove errors associated with the antennas, we used an improved free-space calibration process[33] within the Agilent 85071E measurement software. After calibration, the chiral metamaterial sample was placed between the two antennas.

Characterization. Since the signals from the horn antennas were linearly polarized, the transmission coefficients for the linearly polarized waves were measured as T_{xx}, T_{xy}, T_{yx}, and T_{yy}, where the first subscript indicates the polarization (x or y) of the transmitted wave and the second subscript indicates the polarization of the incident

wave. From these transmission coefficients calculated in a linear basis, the right and left circularly polarized transmission (RCP/LCP) coefficients (T_{++}, T_{+-}, T_{-+} and T_{--}) can be obtained[20,22].

Numerical modelling. For the modelling of chiral metamaterials, we employed the FEM solver of the commercially available software package (CST Microwave Studio). In the simulations, the unit cell boundary condition was applied. The dielectric constant and loss tangent of the Teflon board are $\mathrm{Re}(\varepsilon_r) = 2.5$ and $\tan\delta = 0.0019$ and the metallic strips are considered as a perfect electric conductor.

Gap width vs. field enhancement in a metallic straight strip. To verify quantitatively the dependence of the field enhancement on the gap width, the field enhancement was numerically calculated for the various gap widths. The field enhancement factor is defined by $<\mathrm{E_{gap}}>/E_{in}$, where E_{in} and E_{gap} are the electric field amplitudes of the incident field and inside the gap, respectively, and

$$\langle \mathrm{E_{gap}} \rangle = (gt)^{-1} \iint_s E_{gap}\, dS.$$

1. Barron, L. D. *Molecular Light Scattering and Optical Activity,* Cambridge University Press, 2004.4.
2. Hecht, E. *Optics* 4th edn (MA: Addison-Wesley Publishing Company, 2001).
3. Lindell, I. V., Sihvola, A. H., Tretyakov, S. A. & Viitanen, A. J. *Electromagnetic Waves in Chiral and Bi-isotropic Media* (ArtechHouse, Boston, , London, 1994).
4. Rogacheva, A. V., Fedotov, V. A., Schwanecke, A. S. & Zheludev, N. I. Giant gyrotropy due to electromagnetic-field coupling in a bilayered chiral structure. *Phys. Rev. Lett.* **97**, 177401 (2006).
5. Plum, E., Fedotov, V. A. & Zheludev, N. I. Optical activity in extrinsically chiral metamaterial. *Appl. Phys. Lett.* **93**, 191911 (2008).
6. Decker, M. *et al.* Strong optical activity from twisted-cross photonic metamaterials. *Opt. Lett.* **34**, 2501–2503 (2009).
7. Pendry, J. B. A chiral route to negative refraction. *Science* **306**, 1353–1355 (2004).
8. Plum, E. *et al.* Metamaterial with negative index due to chirality. *Phys. Rev. B* **79**, 035407 (2009).
9. Zhang, S. *et al.* Negative refractive index in chiral metamaterials. *Phys. Rev. Lett.* **102**, 023901 (2009).
10. Zhou, J. *et al.* Negative refractive index due to chirality. *Phys. Rev. B* **79**, 121104 (2009).
11. Wiltshire, M. C. K., Pendry, J. B. & Hajnal, J. V. Chiral Swiss rolls show a negative refractive index. *J. Phys.: Condens. Matt.* **21**, 292201 (2009).
12. Zhao, R., Zhou, J., Koschny, Th., Economou, E. N. & Soukoulis, C. M. Repulsive Casimir Force in Chiral Metamaterials. *Phys. Rev. Lett.* **103**, 103602 (2009).
13. Ren, M., Plum, E., Xu, J. & Zheludev, N. I. Giant nonlinear optical activity in a plasmonic metamaterial. *Nature Comm.* **2**, 833 (2012).
14. Zhang, S., Zhou, J., Park, Y.-S., Rho, J., Singh, R., Nam, S., Azad, A. K., Chen, H.-T., Yin, X., Taylor, A. J. & Zhang, X. Photoinduced handedness switching in terahertz chiral metamolecules. *Nature Comm.* **3**, 942 (2012).
15. Zhou, J., Chowdhury, D. R., Zhao, R., Azad, A. K., Chen, H.-T., Soukoulis, C. M., Taylor, A. J. & O'Hara, J. F. Terahertz chiral metamaterials with giant and dynamically tunable optical activity. *Phys. Rev. B.* **86**, 035448 (2012).
16. Helgert, C. *et al.* Chiral metamaterial composed of three-dimensional plasmonic nanostructures. *Nano Lett.* **11**, 4400–4404 (2011).
17. Gansel, J. K. *et al.* Gold helix photonic metamaterial as broadband circular polarizer. *Science* **325**, 1513–1515 (2009).
18. Wu, C. *et al.* Metallic helix array as a broadband wave plate. *Phys. Rev. Lett.* **107**, 177401 (2011).
19. Zhao, Y., Belkin, M. A. & Alù, A. Twisted optical metamaterials for planarized ultrathin broadband circular polarizers. *Nature Comm.* **3**, 870 (2012).
20. Zhao, R., Zhang, L., Zhou, J., Koschny, T. & Soukoulis, C. Conjugated gammadion chiral metamaterial with uniaxial optical activity and negative refractive index. *Phys. Rev. B* **83**, 035105 (2011).
21. Li, Z. *et al.* Chiral metamaterials with negative refractive index based on four "U" split ring resonators. *Appl. Phys. Lett.* **97**, 081901 (2010).
22. Wang, B. *et al.* Chiral metamaterials: simulations and experiments. *J. Opt. A: Pure Appl. Opt.* **11**, 114003 (2009).
23. Kenanakis, G. *et al.* Flexible chiral metamaterials in the terahertz regime: a comparative study of various designs. *Opt. Mat. Express* **2**, 1702–1712 (2012).
24. Choi, M. *et al.* A terahertz metamaterial with unnaturally high refractive index. *Nature* **470**, 369–373 (2011).
25. Seo, M. *et al.* Terahertz field enhancement by a metallic nano slit operating beyond the skin-depth limit. *Nat. Photonics* **3**, 152–156 (2009).
26. Zhou, J. *et al.* Unifying approach to left-handed material design. *Opt. Lett.* **31**, 3620 (2006).
27. Zhao, R., Koschny, T. & Soukoulis, C. M. Chiral metamaterials: retrieval of the effective parameters with and without substrate. *Opt. Express* **18**, 14553–14567 (2010).
28. Sakurai, T. & Tamaru, K. Simple formulas for two- and three-dimensional capacitances. IEEE Trans. *Electron Devices* ED-30, 183–185 (1983).
29. Huang, X.-R., Peng, R.-W., & Fan, R.-H. Making Metals Transparent for White Light by Spoof Surface Plasmons. *Phys. Rev. Lett.* **105**, 243901 (2010).
30. Foteinopoulou, S., Vigneron, J., & Vandenbem, C. Optical near-field excitations on plasmonic nanoparticle-based structures. *Opt. Express* **15**, 4253–4267 (2007).
31. Lei, D. Y., Aubry, A., Maier, S. A. & Pendry, J. B. Broadband nano-focusing of light using kissing nanowires. *New J. Phys.* **12**, 093030 (2010).
32. Hess, O., Pendry, J. B., Maier, S. A., Oulton, R. F., Hamm, J. M. & Tsakmakidis, K. L. Active optical metamaterials. *Nature Materials* **11**, 573 (2012).
33. Bartley, P. G. & Begley, S. B. Improved Free-Space S-Parameter Calibration. *Instrumentation and Measurement Technology Conference, 2005. IMTC 2005— Proceedings of the IEEE* **1**, 372 (2005).

Author contributions

T.-T.K., S.S.O., W.C., O.H. and B.M. conceived the original idea. T.-T.K. performed the numerical simulation and the microwave measurement. T.-T.K. and H.-S.P. fabricated the samples and measured THz optical properties. S.S.O., R.Z., S.-H.K. and O.H. developed the analytical model. All the authors analysed the data and wrote the manuscript.

Additional information